Biosensors and Bioelectronics 198 (2022) 113826

Contents lists available at ScienceDirect

Biosensors and Bioelectronics

journal homepage: www.elsevier.com/locate/bios

The activity of alkaline phosphatase in breast cancer exosomes simplifies the biosensing design

Silio Lima Moura [a], Arnau Pallarès-Rusiñol [a,b], Luciano Sappia [a], Mercè Martí [b], María Isabel Pividori [a,b,*]

[a] Grup de Sensors i Biosensors, Departament de Química, Universitat Autònoma de Barcelona, 08193, Bellaterra, Spain
[b] Biosensing and Bioanalysis Group, Institute of Biotechnology and Biomedicine, Universitat Autònoma de Barcelona, Bellaterra, 08193, Spain

ARTICLE INFO

Keywords:
Exosomes
Alkaline phosphatase
Breast cancer
Liquid biopsy
Immunomagnetic separation
Electrochemical biosensor

ABSTRACT

This work addresses a biosensor combining the immunomagnetic separation and the electrochemical biosensing based on the intrinsic ALP activity of the exosomes. This approach explores for the first time two different types of biomarkers on exosomes, in a unique biosensing device combining two different biorecognition reaction: immunological and enzymatic. Besides, the intrinsic activity of alkaline phosphatase (ALP) in exosomes as a potential biomarker of carcinogenesis as well as osseous metastatic invasion is also explored. To achieve that, as an *in vitro* model, exosomes from human fetal osteoblasts are used. It is demonstrated that the electrochemical biosensor improves the analytical performance of the gold standard colorimetric assay for the detection of ALP activity in exosomes, providing a limit of detection of 4.39 mU L^{-1}, equivalent to 10^5 exosomes μL^{-1}. Furthermore, this approach is used to detect and quantify exosomes derived from serum samples of breast cancer patients. The electrochemical biosensor shows reliable results for the differentiation of healthy donors and breast cancer individuals based on the immunomagnetic separation using specific epithelial biomarkers CD326 (EpCAM) combined with the intrinsic ALP activity electrochemical readout.

1. Introduction

Alkaline phosphatases (ALP, EC 3.1.3.1) are a family of ubiquitous enzymes present in most tissues. These membrane-bound metalloenzymes catalyze the hydrolysis of phosphate monoesters in an alkaline medium into inorganic phosphate and its corresponding alcohol (Sharma et al., 2014; Tang et al., 2019). Each active site of the enzymes contains two Zn^{2+} and one Mg^{2+} metallic-ions binding sites, necessary for the folding of the enzyme and the binding of phosphate groups (Dean, 2002; Sowadski et al., 1981). ALP are key enzymes involved in multiple biological and metabolic pathways, including the bone mineralization process, which increases the local concentration of phosphate ions (Anderson, 2003) by consuming pyrophosphate from the medium, known as inhibitor of the formation of hydroxyapatite crystals (Anderson et al., 2004).

In this sense, the ALP activity is a well-established biomarker, routinely determined in clinical analysis, for the monitoring of a series of diseases. For example, ALP plays a role in bile production and in the diagnosis of liver disorders, the assessment of its enzymatic activity is a key parameter because particular patterns of liver enzymes activity can be linked to common diseases (Giannini et al., 2005). It is also found that high levels of ALP in human saliva can be indicative of periodontal disease (Luke et al., 2015; Melguizo-Rodríguez et al., 2020).

Besides the abovementioned, several studies have demonstrated that the overexpression of ALP can be correlated with metastatic processes in cancer disease, such as osteosarcoma (Kim et al., 2017), prostate (Rao et al., 2017), breast (Tsai et al., 2000) and colorectal carcinomas (Saif et al., 2005).

The standard method for ALP activity determination in clinical fluids is based on a spectrophotometric assay, in which the sample is mixed with an alkaline buffer and a substrate (para-nitrophenyl phosphate), and measuring the product at 405 nm (Keiding et al., 1974). This substrate is also widely used in electrochemical biosensors (Akyilmaz and Turemis, 2010). Recently, our group reported an electrochemical biosensor for the determination of ALP in clinical samples (Sappia et al., 2019). We also demonstrated ALP activity on osteoblast-derived

* Corresponding author. Grup de Sensors & Biosensors, Unitat de Química Analítica, Universitat Autònoma de Barcelona, Edificio Cn. Campus UAB, 08193, Bellaterra, Barcelona, Spain.
E-mail address: isabel.pividori@uab.cat (M.I. Pividori).

https://doi.org/10.1016/j.bios.2021.113826
Received 18 October 2021; Received in revised form 16 November 2021; Accepted 19 November 2021
Available online 23 November 2021

exosomes from culture supernatants (Sanchez et al., 2020).

The exosomes are nano-sized extracellular vesicles involved in intercellular communication mechanisms (Johnstone et al., 1987). The exosome cargo is derived from the producing cells and includes tetraspanins (e.g. CD9, CD63, CD81 considered as ubiquitous exosome markers), DNA, RNA but also enzymes of cellular origin (Samanta et al., 2018). Exosomes are currently under study as biomarkers for cancer diagnosis and monitoring (Halvaei et al., 2018; Raposo and Stoorvogel, 2013; Zhou et al., 2021). Most of the studies of exosome detection involving biosensors use antibodies for the specific capturing and detection, for the discrimination of the cellular origin of the exosomes (Liu et al., 2021; Moura et al., 2020a, 2020b). Even though, the heterogeneity of the exosomes can impair the use of a good antibody pair for capture and detection with high specificity, low background, and no cross-reactivity.

Since there is a correlation among bone metastasis in breast cancer and the increase of alkaline phosphatase in microcalcifications (Du et al., 2014; Kanakis et al., 2004; Zulauf et al., 2019), in this paper we address the use of exosome ALP activity instead of a labeled-antibody to achieve the electrochemical readout. Several methods of ALP measurement are commonly used in clinical practice, but none of them are focused on the analysis of ALP in the serum-derived exosomes from epithelial cancer cells. To our knowledge, this is the first time that the enzymatic activity of exosomes is proposed for the redout in a biosensor.

The method was firstly optimized using an *in vitro* model based on exosomes derived from human fetal osteoblastic (hFOB) cell line and compared with the gold standard colorimetric ALP assay in terms of the analytical performance. In this first approach, the proposed biosensor combines the immunomagnetic separation of the exosomes based on the general tetraspanin (CD9, CD63, or CD81), followed by the electrochemical readout relying on the determination of ALP activity with pNPP substrate by using boron-doped microcrystalline diamond (BDD) electrodes. As a proof of concept in real samples, the biosensing approach was tested to discriminate breast cancer individuals from healthy donors by the analysis of serum samples (Moura et al., 2020a; Soysal et al., 2013). In this instance, the exosomes were isolated using magnetic particles specific for CD326 (EpCAM) cancer-related biomarker, followed by the electrochemical biosensing of ALP content, which differentiates healthy donors and breast cancer patients based on specific epithelial biomarkers.

2. Experimental

2.1. Instrumentation

Nanoparticle tracking analysis (NTA) was performed using the NanoSight LM10-HS system with a tuned 405 nm laser (NanoSight Ltd, UK). Cryogenic transmission electron microscopy (Cryo-TEM) images were collected by a Jeol JEM 2011 (JEOL USA Inc, USA) using an accelerating voltage of 200 kV. Flow cytometry was performed using BD FACSCANTO II (BD Biosciences, USA) equipment. The Media Fluorescence Intensity and beads count data were obtained by FlowJo analysis software of every sample-reading file. Confocal images were collected on the microscope Leica, TCS SP5 (Leica Microsystems, Germany). Optical measurements were performed on a TECAN Infinite m200 PRO (TECAN AG, Switzerland) microplate reader with Magellan v7.0 software. All electrochemical experiments were performed using an AUTOLAB PGSTAT10 potentiostat/galvanostat electrochemical analyzer (Metrohm AG, Switzerland). A boron-doped microcrystalline diamond (BDD) electrode (boron/carbon ratio of 20.000 ppm) as working electrode (geometric area = 0.5 cm^2) was kindly supplied by Prof. Dr. Neidenei Ferreira from Group of Electrochemistry and Carbon Materials, National Institute of Space Research (INPE), São José dos Campos, São Paulo, Brazil. The construction of the BDD electrode is described in Supp. Data S1, as well as the characterization by Scanning Electron Microscopy, RAMAN and Cyclic Voltammetry. Ag/AgCl/$KCl_{(sat.)}$ reference electrode, a disc platinum counter electrode (geometric area = 3.0 cm^2) and a standard 500-μL one compartment three-electrode cell was used in all experiments.

2.2. Chemicals and biochemicals

The magnetic particles (MPs) Dynabeads® M450 Tosylactivated (Ref. 14013) and the MPs modified with EpCAM antibody (Dynabeads™ Epithelial Enrich, Ref. 16102) were purchased from Thermo Fisher. The mouse monoclonal antibodies (antiCDX) were purchased from Thermo Fisher: CD9 (Ref. 10626D), CD63 (Ref. 10628D) and CD81 (Ref. 10630D). A goat anti-mouse IgG H&L (Cy5®) (antimouse-Cy5) (Ref. ab97037) was purchased from Abcam. Calf intestine alkaline phosphatase (ALP, ref. 10713023001), Dulbecco's Modified Eagle's/Ham's F-12 Nutrient (DMEM/F12, nº D9785) medium and fetal bovine serum (FBS, ref. 12007C) were purchased from Sigma-Aldrich. All other reagents were in analytical reagent grade.

2.3. Cell culturing, exosome isolation and purification

Human fetal osteoblastic (hFOB) cell line (hFOB 1.19 ATCC® CRL-11372™) was grown as described in Supp. Data S2. Exosomes were purified from culture supernatant by differential ultracentrifugation as previously reported by our research group (Moura et al., 2020a). Exosomes are resuspended in 10 mmol L^{-1} TRIS buffer solution (pH 7.4) (0.22 μm filtrated and sterile) and stored at –80 °C. All exosomes purification steps are described in Supp. Data S2.

2.4. Characterization of exosomes by nanoparticle tracking analysis and cryogenic transmission electron microscopy

The size distribution and concentration of exosomes were measured by nanoparticle tracking analysis (NTA). The purified exosomes were diluted in sterile-filtered PBS buffer solution (50- to 100-fold). Nanosight NTA Software analyzed raw data videos by triplicate during 60 s with 25 frames/s and the temperature of the laser unit set at 24.8 °C. For the Cryo-TEM, the exosomes (2.0×10^9 exosomes) were directly laid on Formvar-Carbon EM grids and frozen in ethanol. Exosomes were maintained at –182 °C during the whole process.

2.5. Confocal microscopy and flow cytometry study

The analysis of the molecular biomarkers expressed in hFOB cell line was carried out by flow cytometry. The cell-membrane and the exosome expression of CD9, CD63 and CD81 tetraspanins were compared. The indirect labeling of 2×10^5 cells was performed by incubation of 100 μL (5 μg mL^{-1}) of the antibodies antiCDX (mouse), (being CDX either CD9, CD63 and CD81), for 30 min with gentle shaking at 25 °C. After that, three washing steps with TRIS buffer solution containing 0.5% BSA solution were performed. Afterward, 100 μL (2 μg mL^{-1}) of the antimouse-Cy5 antibody (a far-red-fluorescent dye, excitation 647 nm, emission 665 nm) was incubated for 30 min in darkness with gentle shaking at 25 °C. The labeled cells were resuspended in 200 μL of TRIS buffer solution containing 0.5% BSA solution.

The same procedure of labeling was performed in the case of the osteoblast-derived exosomes, but in this approach, and due to their size and resolution of the technique, the exosomes were firstly immobilized on the surface of magnetic particles (MPs). To achieve that, 3.5×10^{10} exosomes were covalently immobilized on 1.6×10^7 MPs, as detailed described in Supp. Data S5 (Fig. S4, panel A), followed by the indirect labeling as described above, with antiCDX (mouse), (being CDX either CD9, CD63 or CD81 biomarkers).

The same samples of cells and exosomes analyzed by flow cytometry were subjected to confocal microscopy imaging for the study of the binding pattern of antibodies. In the case of cells, the cellular DNA was stained previously (before labeling with antibodies) with Hoechst dye (a

blue-fluorescent dye, emission wavelength 490 nm).

2.6. ALP activity study in exosomes

2.6.1. Spectrophotometric determination of the ALP activity in exosomes

The gold standard colorimetric determination of the ALP activity was performed in 96-well microtiter plates (Fig. 1, panel B). The colorimetric assay for ALP activity in osteoblast-derived exosomes was detected and quantified by monitoring the enzymatic activity (rate of micromoles hydrolyzed per minute, μmol min^{-1}) with pNPP substrate in DEA buffer into p-nitrophenol (pNP). A colorimetric calibration curve for pNP was carried out to obtain the rate of hydrolyzing in enzyme activity (U L^{-1}), as described in Supp. Data S12. The assay involved the following steps: i) IMS of the exosomes with antiCDX-MPs (Fig. 1, panel A), followed by ii) reaction with pNPP substrate; iii) optical readout (Fig. 1, panel B). The protocol for the modification of magnetic particles and the spectrophotometric assay are described in detail in Supp. Data S5.2 and S6, respectively.

2.6.2. Electrochemical biosensor for ALP activity in exosomes

The electrochemical biosensing for ALP activity in osteoblast-derived exosomes involved the following steps: i) IMS of the exosomes with antiCDX-MPs (Fig. 1, panel A), followed by ii) reaction with pNPP substrate and (iii) the electrochemical readout (Fig. 1, panel C). The detailed protocol for the electrochemical biosensor is provided in Supp. Data S7. A standard 500-μL one compartment three-electrode cell was used. The readout was performed by monitoring the rate of micromoles hydrolyzed per minute (μmol min^{-1}) of pNPP substrate in DEA buffer into p-nitrophenol (pNP), followed by electrochemical conversion into p-aminophenol (pAP). A square wave voltammetry (SWV) calibration plot for pAP was carried out to express the rate of hydrolyzing in enzyme activity (U L^{-1}), as described in Supp. Data S12.

2.6.3. Electrochemical biosensing of the ALP activity in exosomes isolated by specific epithelial biomarker from serum of breast cancer patients

Blood samples from anonymized healthy female donors (n = 10, mean age 35/SD 5 years) and breast cancer female donors (n = 10, stage IV, mean age 50/SD 6 years) were obtained from the Hospital del Mar, Barcelona, Spain. The work was carried out following the principles of voluntariness and confidentiality. The samples (n = 10) each were pooled in two batches (healthy and breast cancer donors) and purified as detailed described in Supp. Data S2 and S3. The two groups of samples were then evaluated by NTA and the protein content (as described in Supp. Data S4) and compared based on the same content of exosome protein (3.35 μg of protein per assay). The electrochemical biosensing for ALP activity in exosomes from serum of breast cancer patient involved the following steps: i) IMS of the exosomes with antiCD326-MPs (also known as EpCAM, a cancer-related biomarker) in order to isolate only cancer-related exosomes, followed by ii) reaction of the ALP enzyme on the exosomes with pNPP substrate; (iii) electrochemical readout as described above. The detailed protocol for the electrochemical biosensing of the ALP activity in exosomes isolated by specific epithelial biomarker from serum of breast cancer patients is provided in Supp. Data S8.

2.7. Statistical analysis

The statistical analyses were performed using GraphPad Prism 9 (San Diego, USA). The data of the ALP activity were statistically compared between the gold standard colorimetric and the electrochemical endpoint assays using a paired-sample Student's t-test. The value $p > 0.05$ was considered significant.

2.8. Safety considerations

All works were performed in a Biosafety cabinet, and all material was decontaminated by autoclaving or disinfected before discarding following U.S. Department of Health and Human Services guidelines for level 2 laboratory Biosafety.

3. Results and discussion

3.1. Characterization of exosomes by nanoparticle tracking analysis and cryogenic transmission electron microscopy

The diameter size distribution of osteoblast-derived nanovesicles derived from hFOB cell line and human serum samples ranged from 50 up to 460 nm (considering 95.4% of a Gaussian distribution). The highest peaks are enriched with exosomes and correspond to 120–150 nm in diameter (Fig. 2). The NTA profiles observed are characteristic of each sample source, being more heterogenous samples from human serum (Fig. 2, panels B and C). Nevertheless, the particle concentration

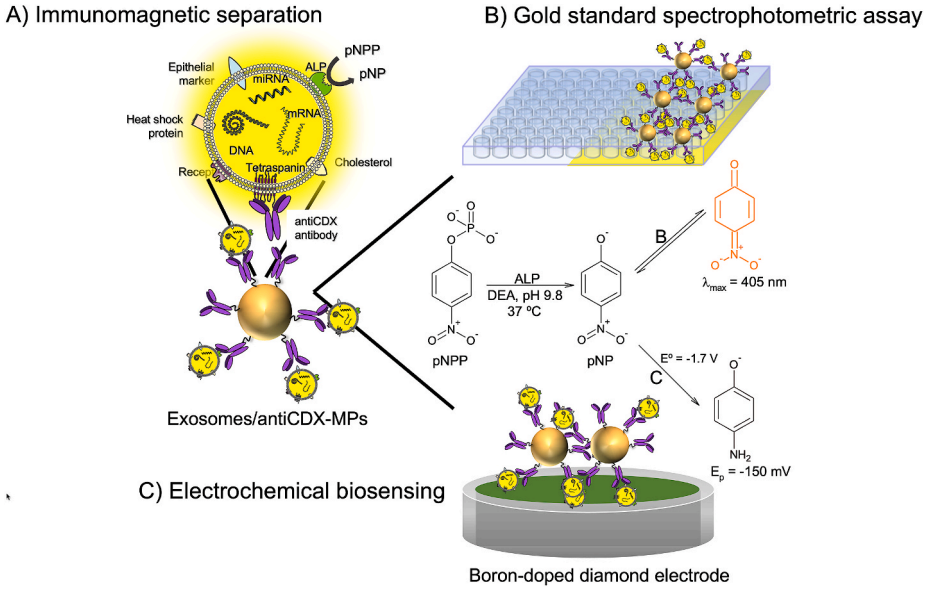

Fig. 1. Different approaches for the detection of alkaline phosphatase (ALP) activity in osteoblast-derived exosomes by optical readout and electrochemical biosensor. Further experimental details are provided in Supp. Data S6 and S7.

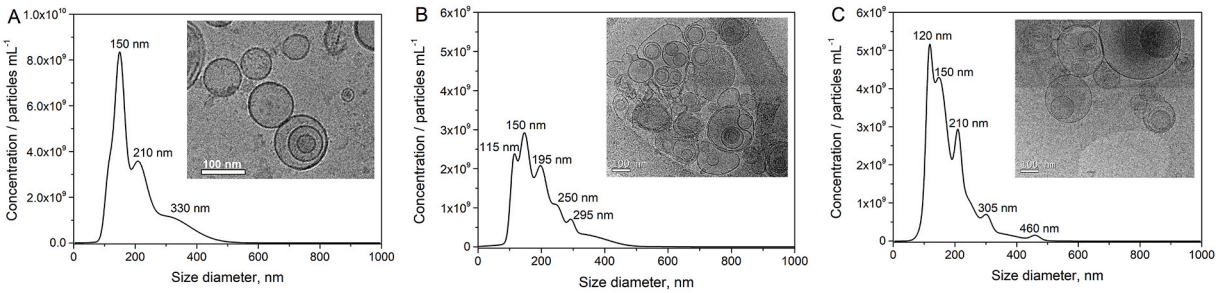

Fig. 2. Characterization by NTA and Cryo-TEM of purified exosomes-derived from hFOB cell line (panel A) and human serum samples from healthy individuals (panel B) and breast cancer patients (panel C). The NTA characterization analyzed raw data videos by triplicate during 60 s with 25 frames per second and the temperature of the laser unit set at 24.8 °C. Cryo-TEM images were obtained at an acceleration voltage of 200 kV.

determined by NTA were similar in all cases, approximately 10^{10} particles mL^{-1}. Further details of NTA characterization are provided in Supp. Data S9.

Cryo-TEM micrographs on osteoblast-derived exosomes show well-shape exosome vesicles with closed circular lipid bilayers (Fig. 2, inset panel A) of around 150 nm in diameter. As expected, the Cryo-TEM micrographs also reveal the presence of some aggregates of exosomes, confirming the results obtained by NTA. In fact, Cryo-TEM micrographs from serum derived exosomes (Fig. 2, insets panels B and C) showed higher aggregation of the vesicles, especially in cancer patient sample, according to the NTA profiles (more micrographs in Supp. Data S9). Finally, it is important to highlight that NTA analysis provides information as counted entities, not only as isolated particles but also as aggregates. Therefore, the NTA analysis cannot clearly distinguish vesicles and vesicle aggregates.

3.2. Confocal microscopy

The expression of general exosome biomarkers such as CD9, CD63 and CD81 not always correlates between cell and exosome membranes. Therefore, the characterization of the expression of those molecules was performed on the hFOB cell line, as well as in their osteoblast-derived exosomes for their further use in the immunomagnetic separation of the exosomes.

Expression patterns to CD9, CD63 and CD81 tetraspanins in hFOB cell line and their exosomes were evaluated qualitatively by confocal microscopy. In the case of hFOB cells, the cellular DNA was stained with Hoechst dye (blue color). CD9, CD63, and with highlight the CD81 tetraspanins membrane receptors are shown with strong labeling in the hFOB cell line (Fig. 3, panel A and C). The percentage of labeled cells represents the total counting of positive cells for each biomarker, as shown in Fig. 3, panel C. The expression of osteoblast-derived exosomes was done after covalent immobilization on MPs due to their size (Fig. S4, panel A) and was then studied and compared to the parental cell line (Fig. 3, panel B). It is worth mentioning that the intense green color is due to autofluorescence on the MPs at 580 nm, approximately (Agrawal et al., 2007). The percentage of labeled exosomes represents the total counting of positive exosomes-MPs for each biomarker. The quantitative analysis showed, as expected, a strong labeling pattern of osteoblast-derived exosomes to all the general tetraspanins studied (CD9, CD63, and CD81) (Fig. 3, panel C).

The results for flow cytometry analysis are shown in Fig. 4. It is noteworthy that the flow cytometric analysis was performed with the same batch sample used in the confocal microscopy. The negative control, in which the signal appears onto the left side in blue, confirms that there is a negligible (<0.1%) nonspecific adsorption of the secondary antibody (antimouse Cy®5 fluorophores) on the hFOB cells (Fig. 4, panel A, control). Flow cytometry also showed strong labeling to CD9, CD63, and CD81 biomarkers in hFOB cell line. The results of flow cytometry shown in Fig. 4, panel B and C, for the osteoblast-derived exosomes covalently immobilized on MPs also confirmed the high level of expression of CD9, CD63, and CD81 tetraspanins (Fig. 4, panel B and C). The percentage of labeled entities (either the cells or the exosomes-MPs) represents the total counting of positive entities for each biomarker, as shown in Fig. 4, panel C.

As for hFOB cells, the CD81 tetraspanin was most prominently displayed in their derived exosomes. In agreement with several studies, CD9, CD63, and CD81 as the most frequently identified proteins in exosomes and are considered classical biomarkers for exosomes (Chow et al., 2014). Therefore, any of these tetraspanins can provide good performance for the immunomagnetic separation of osteoblast-derived exosomes.

3.3. Determination of ALP activity

Different parameters were optimized, and the results shown in Supp. Data S10, including the composition of the buffer (Tris or DEA), pH, Mg^{2+} concentration and the stop solution for ALP activity determination on osteoblast-derived exosomes. According to the results, the optimized parameters for the spectrophotometric determination of the ALP activity

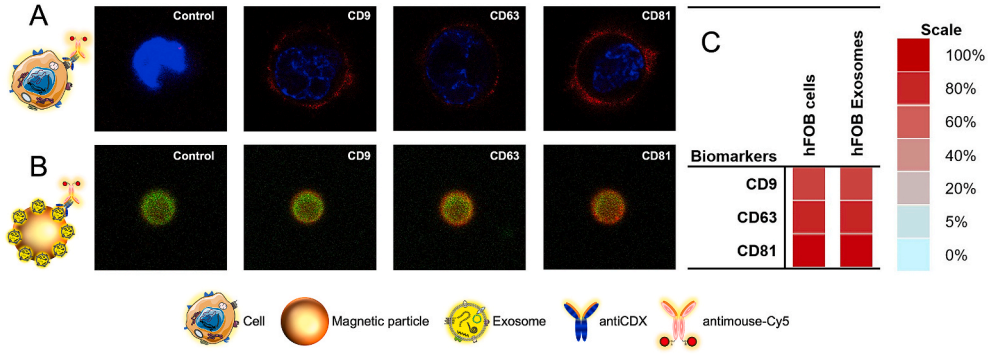

Fig. 3. Confocal microscopy images for (A) hFOB cell line and (B) their exosomes covalently immobilized on MPs (exosomes-MPs), followed by indirect labeling with mouse antiCDX (5 μg mL^{-1}), (being CDX either CD9, CD63, and CD81 biomarkers) and antimouse-Cy5 (2 μg mL^{-1}). The concentration of MPs and exosomes were set in 1 × 10^6 MPs and 4 × 10^9 exosomes per assay, respectively. DNA in blue color, magnetic particles in green color, exosome protein membrane in red color. (For interpretation of the references to color in this figure legend, the reader is referred to the Web version of this article.)

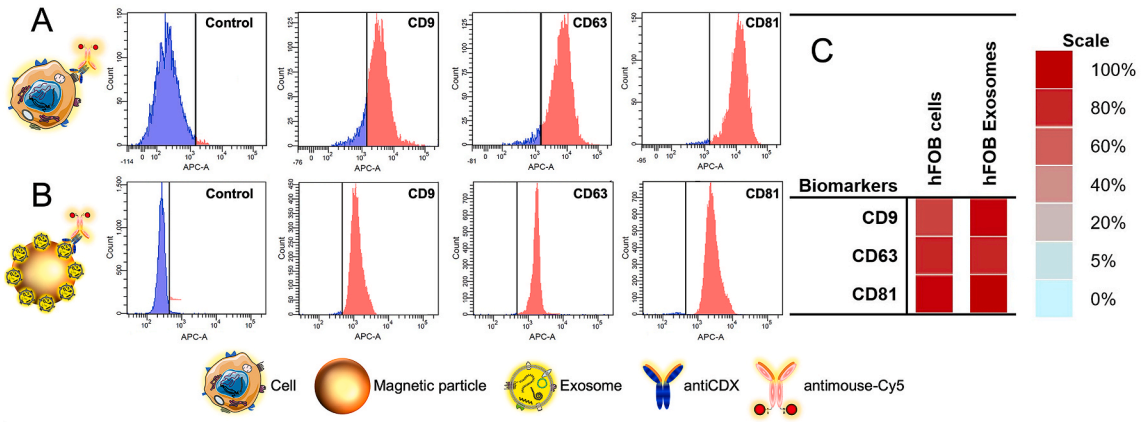

Fig. 4. Flow cytometry study represented in histograms for (A) hFOB cell line and (B) their exosomes covalently immobilized on MPs (exosomes-MPs), followed by indirect labeling with mouse antiCDX (5 μg mL^{-1}), (being CDX either CD9, CD63, and CD81 biomarkers) and antimouse-Cy5 (2 μg mL^{-1}). The concentration of MPs and exosomes were set in 1×10^6 MPs and 4×10^9 exosomes per assay, respectively. Population control onto the stained-blue regions on the left side and stained-red regions on the right side for a positive relative expression of membrane protein markers. (For interpretation of the references to color in this figure legend, the reader is referred to the Web version of this article.)

in osteoblast-derived exosomes immunocaptured by antiCDX-MPs were 10 mmol L^{-1} pNPP in 1 mol L^{-1} DEA buffer (pH 9.8) containing 6.0 mmol L^{-1} $MgCl_2$ and 100 mmol L^{-1} KCl. In all cases, the enzymatic reaction was performed for 60 min at 37 °C and stopped by adding 25% (v/v) of 5.0 mol L^{-1} NaOH, and finally, the absorbance was measured at 405 nm. (Supp. Data S10).

Beside the characterization of BDD electrode by SEM and Raman, the SWV-parameters were also optimized (Supp. Data S11). The optimal experimental SWV-parameters for quantification of pAP in 1 mol L^{-1} DEA buffer (pH 9.8) containing 6.0 mmol L^{-1} $MgCl_2$ and 100 mmol L^{-1} KCl using microcrystalline BDD electrode were found to be E_{sw} = 200 mV pulse amplitude, = 200 Hz frequency, E_{sp} = 8 mV pulse potential, E_{ap} = -1.70 V and t = 10 s for accumulation potential and time, respectively. Under these conditions, an excellent reproducibility was achieved for the electrochemical readout, as also shown in Supp. Data S11. The substrate also showed a good stability on the BDD electrode (Supp. Data S11).

3.4. Comparative study of the electrochemical biosensor and the spectrophotometric determination for ALP activity in exosomes isolated on magnetic particles

The ALP activity from osteoblast-derived exosomes was detected and quantified by the gold standard spectrophotometric assay by monitoring the absorbance at 405 nm, and the analytical performance compared with the electrochemical biosensing monitoring the current peak at -150 mV. Fig. 5, panel A (spectrophotometric determination) and panel B (electrochemical biosensing) show the ALP activity of osteoblast-derived exosomes isolated by immunomagnetic separation base on antiCDX-MPs (being CDX: CD9, CD63 and CD81). These results demonstrated an improved separation performance of the IMS based on antiCD81-MPs and in the detection of ALP activity in the exosome membrane, which can be attributed either to high expression of the receptor or higher affinity constant (K_a) of the antibody.

Both set of data were fitted using nonlinear regression (Four Parameter Logistic Equation, GraphPad Prism Software). The osteoblast-derived exosomes separated by using antiCD81-MPs provided improved analytical performance, giving a limit of detection (LOD) of 825 exosomes μL^{-1} (r^2 = 0.9907) and 105 exosomes μL^{-1} (r^2 = 0.9949) for spectrophotometric assay and electrochemical biosensor, respectively. The LOD for the electrochemical biosensor corresponds to the 4.39 mU L^{-1} or 13.47 mU mg^{-1} for ALP activity and specific activity, normalized by the protein content, respectively. These LOD represent an improvement over the detection limits obtained by other methods for total exosome counting (López-Cobo et al., 2018; Oliveira-Rodríguez et al., 2016). These results demonstrate a more sensitive electrochemical platform than the gold standard spectrophotometric assay ($p < 0.05$). Nonetheless, the pNPP substrate solution on the BDD electrode surface

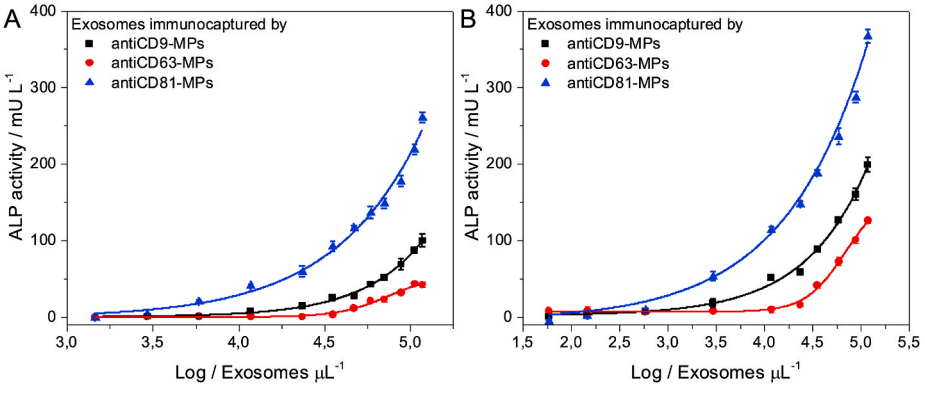

Fig. 5. Comparative study of (A) spectrophotometric gold standard determination and (B) electrochemical biosensor for the detection of ALP activity in osteoblast-derived exosomes ranging 0 from 2.35 × 10^7 exosomes μL^{-1} in 10 mmol L^{-1} TRIS buffer. Exosomes were immunocaptured by antiCDX-MPs (being CDX any of CD9, CD63, or CD81), followed by reaction with 10 mmol L^{-1} pNPP in 1 mol L^{-1} DEA buffer, containing 6.0 mmol L^{-1} $MgCl_2$ and 100 mmol L^{-1} KCl. In all cases, the enzymatic reaction was during 60 min at 37 °C, the concentration of antiCDX-MPs was fixed in 1 × 10^6 MPs. An enzymatic colorimetric assay was monitored at 405 nm and the electrochemical signal monitored the current peak at -150 mV vs. Ag/AgCl/$KCl_{(satd.)}$. BDD electrode was used as a working electrode. SWV conditions: E_{sw} = 200 mV, E_{ap} = -1.70 V, E_{sp} = 8 mV, f = 200 Hz, t = 10 s, in a potential window from -0.4 to 0.1 V. Further details of the conversion of absorbance and current into ALP enzymatic activity are provided in Supp. Data S12. The error bars show the standard deviation for n = 3. (For interpretation of the references to color in this figure legend, the reader is referred to the Web version of this article.)

has an excellent hydrolytic stability with no formation of pNP/pAP, remaining colorless in absence of ALP enzyme (Fig. S14, Supp. data).

Previous studies reported the monitoring of ALP activity in human serum using a glassy carbon electrode by the rate of hydrolysis of ascorbic acid 2- phosphate (AAP) (Sun and Jiao, 2005). ALP enzymatic hydrolysis product of AAP produced ascorbic acid (AA), which was monitored at 0.38 V (vs Ag/AgCl/KCl$_{(sat.)}$) by using differential pulse voltammetric (DPV) and ALP assay exhibited a LOD of 0.3 U L^{-1}. Although a broad operating range (0.4–2000 U L^{-1}) was covered as mentioned by the authors, the use of carbon electrode needs of a mechanical polishing and the spontaneous oxidation of the enzymatic product ascorbic acid in presence of atmospheric air turn the assay into not appropriate for implementation as a portable system for ALP activity determination. Nonetheless, the ascorbic acid undergoes oxidation at 0.38 V (vs Ag/AgCl/KCl$_{(sat.)}$), which is a high potential, not desirable and relatively complicated in the determination of an electroactive analyte due to possible interfering molecules. This probably happens in the same way as in the dimerization of aniline (Sapurina et al., 2015) and dapsone (Moura et al., 2015). Other researchers have addressed the electrochemical determination of ALP activity using indium–tin oxide (ITO) electrode (Qin et al., 2017), graphite screen-printed electrode (Sappia et al., 2019), graphite-IrO2 composites (Wang et al., 2009), graphene oxide-modified gold electrode (Shen et al., 2016), copper sulfide-decorated graphene sheet (Peng et al., 2015). Although these works and others reported in the literature have demonstrated advances in the strategy towards ALP-based assays, some drawbacks are crucial in the ALP determination as to the cost-effectiveness, non-reusable and electrode surface fouling, high potential detection to phenolic-type substrates, which current peaks overlap with the oxygen-evolution region (>1.0 V vs. Ag/AgCl/KCl$_{(sat.)}$).

3.5. *Electrochemical biosensing of the intrinsic activity of ALP in exosomes isolated by specific epithelial biomarker from serum of breast cancer patients*

The analysis of purified exosomes from healthy donors and breast cancer patients is shown in Fig. 6. The approach is based on the immunomagnetic separation of the exosomes using the specific CD326 (also known as EpCAM) cancer-related biomarker, followed by the detection of exosome-derived ALP enzyme by reaction with pNPP substrate.

Accordingly, and to compare the expression of the receptors on exosomes from the two populations, the electrochemical biosensing was performed with the same amount (3.35 μg) of exosome protein content per assay, for healthy donors and breast cancer patients (n = 10 each). Fig. 6, shows that breast cancer patients overexpressed ALP enzyme in CD326-positive exosomes and can be well discriminated from exosome-derived healthy donors (mean 4.5-fold, $p < 0.05$), without the need of a secondary labelling antibody for detection of the vesicles.

4. Conclusion

To the best of the author's knowledge, this is the first electrochemical biosensor approach integrating the magnetic particles specific isolation to the detection of ALP activity, both in osteoblast-derived and breast cancer exosomes. This approach demonstrated to be useful for the discrimination of healthy and breast cancer patient, confirming the simultaneous expression of cancer biomarkers in exosomes, as is the case of epithelial CD326 (EpCAM), used for the specific isolation, and the ALP intrinsic activity, used for the sensitive electrochemical readout. The ALP-based electrochemical biosensor for exosomes with a limit of detection of 10^5 exosomes μL^{-1} (4.39 mU L^{-1} or 13.47 mU mg^{-1}) represents an improvement in LODs regarding other exosome quantification (Xia et al., 2017; Yadav et al., 2017), and is more sensitive than the gold standard spectrophotometric assay. The low monitored potential of -150 mV vs. Ag/AgCl/KCl$_{(sat.)}$ avoids possible interfering molecules.

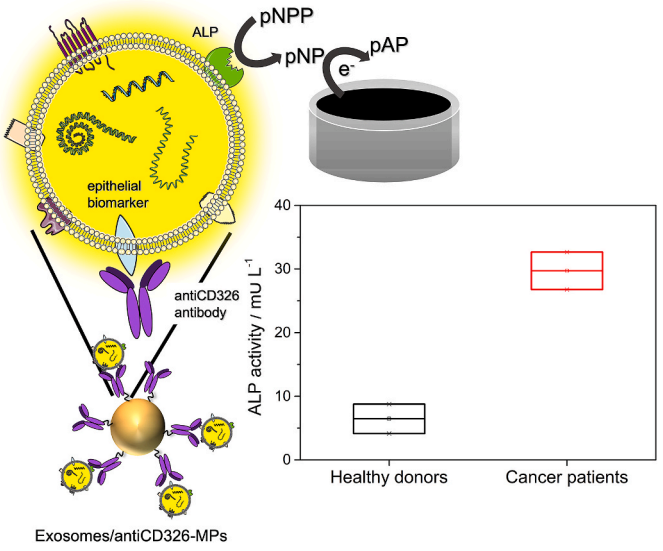

Fig. 6. Electrochemical biosensing for detection of the ALP activity from purified exosomes derived from healthy donors (n = 10, pooled) and breast cancer (n = 10, pooled) patients. The exosomes were preconcentrated on the surface of the electrode by immunomagnetic separation based on antiCD326-MPs (1×10^6 MPs per assay), followed by reaction with 10 mmol L^{-1} pNPP in 1 mol L^{-1} DEA buffer, containing 6.0 mmol L^{-1} $MgCl_2$ and 100 mmol L^{-1} KCl. The electrochemical signal monitored the current peak at -150 mV *vs.* Ag/AgCl/KCl$_{(satd.)}$. BDD electrode was used as a working electrode. SWV conditions: E_{sw} = 200 mV, E_{ap} = -1.70 V, E_{sp} = 8 mV, f = 200 Hz, t = 10 s, in a potential window from -0.4 to 0.1 V. In all cases, the enzymatic reaction was during 120 min at 37 °C. Further details of the conversion of current in ALP enzymatic activity are provided in Supp. Data S12.

These advantages are attributed to the conductivity, stability, very low adsorption, and excellent catalytic properties of the boron-doped diamond (BDD) electrode for ALP determination. Furthermore, the use of a boron-doped microcrystalline diamond (BDD) electrode enables the sample volume minimization, preventing the fouling of nitro-phenolic derivatives, an effect usually observed in conventional-based electrodes (Sappia et al., 2019). Furthermore, this approach simplified the conventional sandwich immunosensing format, which uses two antibodies for the detection, and in most of the instances, two incubation and a further enzymatic reaction (Moura et al., 2020a, 2020b). The difference among healthy donors and breast cancer patients is in accordance with the highly expressed epithelial biomarker CD326 previously reported by our research group (Moura et al., 2020a, 2020b) and ALP enzyme in breast cancer patients (Chen et al., 2017; Tsai et al., 2000; Zulauf et al., 2019; Sanchez et al., 2020). Although this is a preliminary study, the proposed biosensing approach, which combines the exosome immunocapture and the intrinsic enzymatic detection, provides a new device aimed at the simplification of the analytical procedure. In the case of nanovesicles with multiple biomarkers, the need of two or more antibodies for capturing and detection implies expensive and time-consuming assays to find a good antibody pair while avoiding cross-reactivity. Moreover, some subpopulation can be excluded since the two biomarkers should be equally expressed in a single exosome. The use of the intrinsic enzymatic activity of the vesicles is a novel strategy that can be applied in other devices not only for the electrochemical readout, but also with visual detection in paper-based RDTs using the proper substrates for ALP activity.

CRediT authorship contribution statement

Silio Lima Moura: Data curation, Investigation, Validation, Writing – original draft. **Arnau Pallarès-Rusiñol:** Visualization, Formal analysis, Writing – original draft. **Luciano Sappia:** Investigation, Validation.

Mercè Martí: Conceptualization, Methodology, Supervision. **María Isabel Pividori:** Conceptualization, Methodology, Supervision, Funding acquisition.

Declaration of competing interest

The authors declare that they have no known competing financial interests or personal relationships that could have appeared to influence the work reported in this paper.

Acknowledgments

This work was funded by the Ministry of Economy and Competitiveness, Madrid (Project BIO2016-75751-R), and Ministry of Science and Innovation (Project PID2019-106625RB-I00). Also, Ministry of Universities (Grant FPU16/01579) and CNPq – Conselho Nacional de Desenvolvimento Científico e Tecnológico, of the Ministry of Science, Technology, Innovation and Communications of Brazil (CNPq/CsF – 233595/2014-7) are gratefully acknowledged.

Appendix A. Supplementary data

Supplementary data to this article can be found online at https://doi.org/10.1016/j.bios.2021.113826.

References

Agrawal, A., Sathe, T., Nie, S., 2007. J. Agric. Food Chem. 55, 3778–3782.
Akyilmaz, E., Turemis, M., 2010. Electrochim. Acta 55, 5195–5199.
Anderson, H.C., 2003. Matrix vesicles and calcification. Curr. Rheumatol. Rep. 5, 222–226.
Anderson, H.C., Sipe, J.B., Hessle, L., Dhamyamraju, R., Atti, E., Camacho, N.P., Millán, J.L., 2004. Am. J. Pathol. 164, 841–847.
Chen, W.-Z., Shen, J.-F., Zhou, Y., Chen, X.-Y., Liu, J.-M., Liu, Z.-L., 2017. Sci. Rep. 7, 11325.
Chow, A., Zhou, W., Liu, L., Fong, M.Y., Champer, J., Van Haute, D., Chin, A.R., Ren, X., Gugiu, B.G., Meng, Z., Huang, W., Ngo, V., Kortylewski, M., Wang, S.E., 2014. Sci. Rep. 4, 5750.
Dean, R.L., 2002. Biochem. Mol. Biol. Educ. 30, 401–407.
Du, W.X., Duan, S.F., Chen, J.J., Huang, J.F., Yin, L.M., Tong, P.J., 2014. J. Cancer Res. Therapeut. 10, C140–C143.
Giannini, E.G., Testa, R., Savarino, V., 2005. CMAJ (Can. Med. Assoc. J.) 172, 367–379.
Halvaei, S., Daryani, S., Eslami-S, Z., Samadi, T., Jafarbeik-Iravani, N., Bakhshayesh, T. O., Majidzadeh-A, K., Esmaeili, R., 2018. Mol. Ther. Nucleic Acids 10, 131–141.
Johnstone, R.M., Adam, M., Hammond, J.R., Orr, L., Turbide, C., 1987. J. Biol. Chem. 262, 9412–9420.
Kanakis, I., Nikolaou, M., Pectasides, D., Kiamouris, C., Karamanos, N.K., 2004. J. Pharmaceut. Biomed. Anal. 34, 827–832.
Keiding, R., Hörder, M., Denmark, W.G., Pitkänen, E., Tenhunen, R., Strömme, J.H., Theodorsen, L., Waldenström, J., Tryding, N., Westlund, L., 1974. Scand. J. Clin. Lab. Invest. 33, 291–306.
Kim, S.H., Shin, K.H., Moon, S.H., Jang, J., Kim, H.S., Suh, J.S., Yang, W.I., 2017. Cancer Med. 6, 1311–1322.
Liu, C., Qie, Y., Qin, W., Zhao, K., Zhu, J., Zhao, L., Li, M., Guo, L.H., 2021. Sensor. Actuator. B Chem. 345, 130336.
López-Cobo, S., Campos-Silva, C., Moyano, A., Oliveira-Rodríguez, M., Paschen, A., Yáñez-Mó, M., Blanco-López, M.C., Valés-Gómez, M., 2018. J. Nanobiotechnol. 16, 47.
Luke, R., Khan, S.N., Iqbal, P.S., Soman, R.R., Chakkarayan, J., Krishnan, V., 2015. J. Int. Oral Health 7, 54–57.
Melguizo-Rodríguez, L., Costela-Ruiz, V.J., Manzano-Moreno, F.J., Ruiz, C., Illescas-Montes, R., 2020. Int. J. Mol. Sci. 21, 1–17.
Moura, S.L., Martín, C.G., Martí, M., Pividori, M.I., 2020a. Talanta 211, 120657.
Moura, S.L., Martín, C.G., Martí, M., Pividori, M.I., 2020b. Biosens. Bioelectron. 150, 111882.
Moura, S.L., Santos Júnior, J.R. Dos, MacHado, F.B.C., Kawachi, E.Y., Ferrão, L.F.D.A., 2015. J. Electroanal. Chem. 757, 230–234.
Oliveira-Rodríguez, M., López-Cobo, S., Reyburn, H.T., Costa-García, A., López-Martín, S., Yáñez-Mó, M., Cernuda-Morollón, E., Paschen, A., Valés-Gómez, M., Blanco-López, M.C., 2016. J. Extracell. Vesicles 5, 31803.
Peng, J., Han, X.X., Zhang, Q.C., Yao, H.Q., Gao, Z.N., 2015. Anal. Chim. Acta 878, 87–94.
Qin, S., Wang, K., Ma, X., Xiong, W., Yue, Z., Chen, M., 2017. Int. J. Electrochem. Sci. 12, 8908–8917.
Rao, S.R., Snaith, A.E., Marino, D., Cheng, X., Lwin, S.T., Orriss, I.R., Hamdy, F.C., Edwards, C.M., 2017. Br. J. Cancer 116, 227–236.
Raposo, G., Stoorvogel, W., 2013. J. Cell Biol. 200, 373–383.
Saif, M.W., Alexander, D., Wicox, C.M., 2005. J. Appl. Res. Clin. Exp. Therapeut. 5, 88–95.
Samanta, S., Rajasingh, S., Drosos, N., Zhou, Z., Dawn, B., Rajasingh, J., 2018. Acta Pharmacol. Sin. 39, 501–513.
Sanchez, M.A., Felice, B., Sappia, L.D., Lima Moura, S., Martí, M., Pividori, M.I., 2020. Mater. Sci. Eng. C 115, 110931.
Sappia, L., Felice, B., Sanchez, M.A.A., Martí, M., Madrid, R., Pividori, M.I., Pividori, I., 2019. Sensor. Actuator. B Chem. 281, 221–228.
Sapurina, I., Tenkovtsev, A.V., Stejskal, J., 2015. Polym. Int. 64, 453–465.
Sharma, U., Pal, D., Prasad, R., 2014. Indian J. Clin. Biochem. 29, 269–278.
Shen, C., Li, X., Rasooly, A., Guo, L., Zhang, K., Yang, M., 2016. Biosens. Bioelectron. 85.
Sowadski, J.M., Foster, B.A., Wyckoff, H.W., 1981. J. Mol. Biol. 150, 245–272.
Soysal, S.D., Muenst, S., Barbie, T., Fleming, T., Gao, F., Spizzo, G., Oertli, D., Viehl, C.T., Obermann, E.C., Gillanders, W.E., 2013. Br. J. Cancer 108, 1480–1487.
Sun, W., Jiao, K., 2005. Bull. Chem. Soc. Ethiop. 19, 163–173.
Tang, Z., Chen, H., He, H., Ma, C., 2019. TrAC Trends Anal. Chem. (Reference Ed.) 113, 32–43.
Tsai, L.-C., Hung, M.-W., Chen, Y.-H., Su, W.-C., Chang, G.-G., Chang, T.-C., 2000. Eur. J. Biochem. 267, 1330–1339.
Wang, J.H., Wang, K., Bartling, B., Liu, C.C., 2009. Sensors 9, 8709–8721.
Xia, Y., Liu, M., Wang, L., Yan, A., He, W., Chen, M., Lan, J., Xu, J., Guan, L., Chen, J., 2017. Biosens. Bioelectron. 92, 8–15.
Yadav, S., Boriachek, K., Islam, M.N., Lobb, R., Möller, A., Hill, M.M., Hossain, M.S. Al, Nguyen, N.T., Shiddiky, M.J.A., 2017. ChemElectroChem 4, 967–971.
Zhou, S., Yang, Y., Wu, Y., Liu, S., 2021. Anal. Chim. Acta 1175, 338633.
Zulauf, N., Brüggmann, D., Groneberg, D., Oremek, G.M., 2019. Oncology 97, 236–244.